Airborne observations of mercury emissions from the Chicago/Gary urban/industrial area during the 2013 NOMADSS campaign

L.E. Gratz [a, *], J.L. Ambrose [b], D.A. Jaffe [c, d], C. Knote [e], L. Jaeglé [d], N.E. Selin [f], T. Campos [g], F.M. Flocke [g], M. Reeves [g], D. Stechman [g], M. Stell [g], A.J. Weinheimer [g], D.J. Knapp [g], D.D. Montzka [g], G.S. Tyndall [g], R.L. Mauldin III [h], C.A. Cantrell [h], E.C. Apel [g], R.S. Hornbrook [g], N.J. Blake [i]

[a] *Environmental Program, Colorado College, Colorado, CO, USA*
[b] *College of Engineering and Physical Sciences, University of New Hampshire, Durham, NH, USA*
[c] *School of Science, Technology, Engineering, and Mathematics, University of Washington Bothell, Bothell, WA, USA*
[d] *Department of Atmospheric Sciences, University of Washington, Seattle, WA, USA*
[e] *Ludwig-Maximilians-Universität – Lehrstuhl Experimentelle Meteorologie, Munich, Germany*
[f] *Department of Earth, Atmospheric and Planetary Sciences, Massachusetts Institute of Technology, Cambridge, MA, USA*
[g] *National Center for Atmospheric Research, Boulder, CO, USA*
[h] *University of Colorado, Boulder, CO, USA*
[i] *School of Physical Sciences, University of California, Irvine, Irvine, CA, USA*

* Corresponding author.
E-mail address: lgratz@coloradocollege.edu (L.E. Gratz).

1. Introduction

Mercury (Hg) is a bioaccumulative neurotoxin that is primarily introduced to terrestrial and aquatic ecosystems through atmospheric deposition (Driscoll et al., 2013). Annual atmospheric Hg emissions in the U.S. total 52 tons per year (tpy), of which 49% (25.4 tpy) comes from coal combustion for electricity generation (U.S. EPA, 2014a, 2014b). The remainder (26.6 tpy) comes largely from electric arc furnaces for steel manufacturing (~10%), industrial boilers (~7%), and cement manufacturing (~5.5%) with smaller contributions from mercury cell chlor-alkali plants, commercial/industrial solid waste incineration, gold mining, sewage sludge incineration, and mobile sources (U.S. EPA, 2014a, 2014b).

In 2011, the U.S. EPA began regulating Hg emissions from coal-fired power plants (CFPPs) with the Mercury and Air Toxics Standards (MATS), requiring the use of maximum available control technologies for removing Hg from stack emissions (U.S. EPA, 2012). As the utilities began implementing these standards, and in response to earlier regulations of municipal and medical waste incinerators, total U.S. atmospheric emissions declined by 79% from 1990 to 2011 (U.S. EPA, 2014a). Although the U.S. Supreme Court effectively put the MATS on hold in June 2015, arguing that the EPA did not fully consider the costs when implementing these standards, in February 2016 the court allowed the EPA to continue enforcing the MATS while completing a cost-benefit analysis by mid-April 2016 that is now pending review.

Accurately characterizing atmospheric emissions from individual sources and source regions is paramount to effectively mitigating ecosystem Hg contamination. In the U.S., Hg emissions from stationary combustion sources are presumably well-constrained within the national inventories based on stack testing and in light of ongoing regulatory efforts; however, one recent study of total atmospheric Hg (THg) downwind of several major U.S. CFPPs found that inventoried Hg emissions may differ substantially from observed values (Ambrose et al., 2015). Additionally, Hg emissions from other smaller point, area, or mobile sources may be less well characterized given that their individual Hg emissions are lower compared to CFPPs and these sources are not routinely monitored. While the emissions from these individual sources may be small, in places such as heavily industrialized areas their total contribution to local or regional atmospheric Hg may be substantial. It is therefore necessary to validate the emissions inventory with ambient observations. While measurements from a mobile platform are ideal for quantifying the outflow of Hg from major U.S. urban areas, relatively few such studies have been conducted (Radke et al., 2007; Talbot et al., 2008; Weiss-Penzias et al., 2013), and in general airborne observations of atmospheric Hg in the U.S. are limited (Ambrose et al., 2015; Brooks et al., 2014; Gratz et al., 2015; Lyman and Jaffe, 2012; Radke et al., 2007; Swartzendruber et al., 2009; Talbot et al., 2008). This inhibits our ability to fully evaluate the emissions inventory (Weiss-Penzias et al., 2013).

The Chicago, Illinois, and Gary, Indiana, urban/industrial area is one location where a high density of urban emissions and industrial point sources significantly impact local and regional air quality. Atmospheric Hg emissions from Chicago/Gary are largely from coal-fired electricity generation (43%), other fossil fuel electricity generation (11%; includes natural gas, oil, biomass, and other unspecified fossil fuels), and non-ferrous metals processing (11%) (Fig. 1) (U.S. EPA, 2014b). Annual atmospheric Hg emissions from Chicago/Gary have declined from over 3.5 tpy in 2005 (U.S. EPA, 2008), to 1.2 tpy in 2008 (U.S. EPA, 2013), to 0.90 tpy in 2011 (U.S. EPA, 2014b). Outflow of Hg from the Chicago/Gary urban/industrial area significantly contributes to Hg deposition to the Lake Michigan Basin as well as ambient Hg concentrations at downwind surface sites (Gratz et al., 2013a, 2013b; Landis and Keeler, 2002; Landis et al., 2002; Vette et al., 2002). While these earlier studies confirmed regional emissions impacts, they did not examine the accuracy of the emission inventory in detail for the Chicago metropolitan area. Additionally, many published studies of atmospheric Hg in the Lake Michigan Basin were performed prior to the MATS ruling. Because Hg emissions in the region have significantly declined in recent years, it is useful to determine the present impact of Chicago/Gary emissions on the surrounding region.

Here we present airborne observations from the 2013 Nitrogen, Oxidants, Mercury, and Aerosol Distributions, Sources, and Sinks (NOMADSS) campaign of THg, carbon monoxide (CO), nitrogen oxides (NO_x), and sulfur dioxide (SO_2) downwind of the Chicago/Gary urban/industrial area. We combine the airborne data with air mass back-trajectories to identify the outflow plume. We then calculate enhancement ratios (ER) for Hg and the co-pollutants using measurements within the plume, and compare these values to inventoried emission ratios (EmR) from the 2011 U.S. EPA National Emissions Inventory (NEI) to examine the representativeness of the inventory for all Hg emission sectors.

2. Materials and methods

2.1. The NOMADSS campaign

The NOMADSS field campaign took place from June 1 to July 15, 2013 under the umbrella of the Southeast Atmosphere Study (SAS) (http://www.eol.ucar.edu/field_projects/sas). During NOMADSS, we made continuous atmospheric chemical and meteorological measurements on 19 research flights across the southern and eastern U.S. using the National Science Foundation/National Center for Atmospheric Research (NSF/NCAR) C-130 research aircraft. Primary objectives of the NOMADSS Hg research included (1) identifying the mechanism for enhanced oxidized Hg (Hg^{II}) in the free troposphere and (2) constraining the emissions of Hg from major source regions in the eastern U.S. Gratz et al. (2015) and Shah et al. (2016) addressed the first objective. Along with Ambrose et al. (2015) and Song et al. (2016), we address the second objective in the present manuscript. Although we sampled downwind of other major urban areas during NOMADSS, including Indianapolis, Dallas, Houston, and Birmingham, the aircraft performed only a single pass through each of those plumes and, because we are limited by the sampling frequency of our airborne Hg instrument (Section 2.2), we are unable to accurately characterize Hg outflow from those urban areas. We instead focus on Research Flight 15 (RF-15) on July 7, 2013 where we have multiple observations downwind of the Chicago/Gary area.

2.2. Mercury measurements

We measured atmospheric Hg onboard the C-130 using the University of Washington's Detector for Oxidized Mercury Species (DOHGS) (Ambrose et al., 2013, 2015; Lyman and Jaffe, 2012). Ambrose et al. (2015) describe in detail the design and operation of the DOHGS prior to and during NOMADSS. Briefly, the DOHGS simultaneously quantifies THg and gaseous elemental Hg (GEM) at 2.5-min integrated frequency on parallel channels, with Hg^{II} determined as the difference between THg and GEM measurements. We calibrated the DOHGS onboard the C-130 before, during, and after each flight using a custom-built GEM permeation source (Ambrose et al., 2013, 2015; Lyman and Jaffe, 2012). We also calibrated the DOHGS using an $HgBr_2$ permeation source as a proxy for atmospheric Hg^{II} in the laboratory before and after the field campaign (Ambrose et al., 2015). As Hg^{II} concentrations measured over Lake Michigan were below the instrument limit of detection for RF-15 (0.107 ng m^{-3}), we focus only on THg here. We estimate

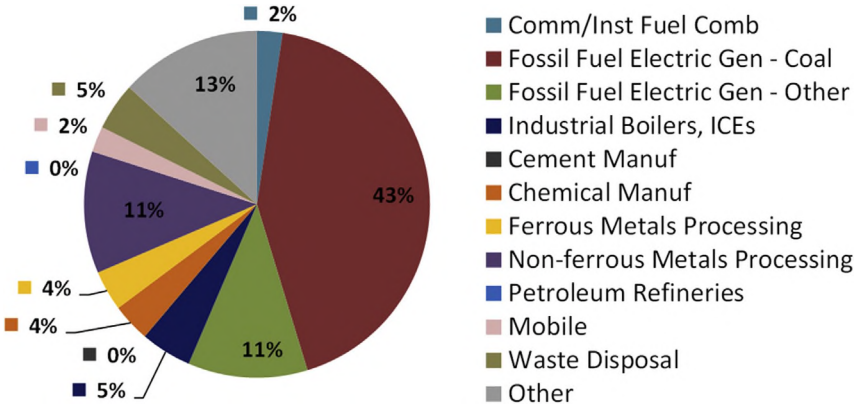

Fig. 1. Mercury emissions by sector for the Chicago/Gary urban area as reported in the 2011 U.S. EPA NEI. Total annual Hg emissions for the Chicago/Gary urban area in the 2011 NEI are 0.90 tons per year (tpy; 1806 lbs yr^{-1}).

the overall uncertainty in THg measurements to be 9.5%, which is the sum in quadrature of the 1σ precision (7.0%) and the systematic (calibration) uncertainty (6.5%) for RF-15 (Ambrose et al., 2015). We converted all THg concentrations to mixing ratios in parts per quadrillion by volume (for GEM, 1 ng m^{-3} at 273.15 K and 1013.25 mbar = 111.73 ppqv).

2.3. Other airborne measurements

We measured nitric oxide (NO) and nitrogen dioxide (NO_2) with a fast-response chemiluminescence instrument at 1-s frequency with uncertainties of 10%, and 15%, respectively (Pollack et al., 2012; Ridley and Grahek, 1990). We report NO_x mixing ratios as the sum of NO and NO_2 and consider the overall NO_x uncertainty to be ±15%. We measured CO in parts per billion by volume (ppbv) at 1-s frequency using an Aero-Laser VUV fluorescence instrument with an overall uncertainty of +(3 ppbv + 5%)/−(3 ppbv + 3%). We measured SO_2 at 10-s frequency using a Thermo Scientific Model 43i-TLE pulse fluorescence gas analyzer with 1σ precision of ±22.5%. We consider the calibration uncertainty in SO_2 measurements to be ±15%. We measured the hydroxyl radical (OH) by chemical ionization mass spectrometry (CIMS) (Mauldin et al., 1998) for 8 out of every 15 s, with values reported as 30-s averages. Overall uncertainty in OH measurements is ±22.5%. We measured volatile organic compounds (VOCs) using the Trace Organic Gas Analyzer (TOGA) at 35-s integrated sampling time (Apel et al., 2015). For the TOGA measurements used here, the overall uncertainty in alkane measurements was ±15% or ±2 pptv (parts per trillion by volume) and for halocarbons was ±10%. Meteorological and state measurements were also collected at 1-s frequency (https://www.eol.ucar.edu/content/nomadss-c-130-documentation).

2.4. FLEXPART

We use the FLEXible PARTicle (FLEXPART) Lagrangian particle dispersion model v9.02 (Stohl et al., 1998, 2005; Stohl and Thomson, 1999) to describe the history of air masses sampled by the C-130. FLEXPART releases a large number of infinitesimally small air parcels (or "particles") from a given location and follows them back in time considering advection, turbulence, and convection (Seibert and Frank, 2004). Deposition and chemical conversion of these "particles" are not considered. Meteorological forcing data are 6-hourly analyses of the National Center for Environmental Prediction (NCEP) Global Forecast System (GFS) on a 0.5° by 0.5° regular grid (http://www.nco.ncep.noaa.gov/pmb/products/gfs/), interlaced with +3 h forecasts.

We apply FLEXPART in two ways: first, we use 72-h air mass back-trajectories generated every 5 min along the C-130 flight track with 1×10^5 particles released to identify when the sampled air mass originated over the Chicago/Gary urban/industrial area (Section 2.5). Second, we apply a "footprint" emission sensitivity analysis to determine the spatial contribution of emissions from the urban/industrial area to the sampled air masses and calculate emission ratios (EmRs) from the 2011 NEI (Section 2.7).

2.5. Measured enhancement ratios (ERs)

We use the back-trajectories and measured enhancements in chemical tracers (THg, NO_x, SO_2, CO, and OH) to determine when the aircraft was within the Chicago/Gary plume. We calculate each THg-based ER (THg/NO_x, THg/SO_2, THg/CO) using 2.5-min averages of 1-s measurements of NO_x, SO_2, and CO during the enhancement period. We also calculate ERs for each combination of co-pollutants (NO_x/CO, SO_2/CO, NO_x/SO_2) using 10-s averages of 1-s measurements. Each ER is the slope of the reduced major axis (RMA) regression. We estimate the uncertainty in each ER as the linear sum of (1) the 95% confidence interval in the RMA regression slope and (2) the sum in quadrature of the calibration uncertainties for the two pollutants (Ambrose et al., 2015).

2.6. Emissions inventory

We obtained annual emissions of Hg, NO_x, SO_2, and CO from the 2011 U.S. EPA NEI (U.S. EPA, 2014b) on a per county basis for point, nonpoint, on road, and nonroad source sectors; we excluded the "events" category (e.g., fires) given their intermittent nature. To define the Chicago/Gary urban/industrial area, we obtained the list of counties incorporated in the Metropolitan Statistical Area (MSA) according to the U.S. Office of Management and Budget (U.S. OMB, 2013). We chose this method because emissions from non-point sources in the U.S. EPA NEI are reported only on a county-wide basis (unlike point source emissions, which are also reported for individual facilities). We then determined the contribution of emissions from these counties to the sampled plume using the FLEXPART footprint analysis (Section 2.7). With this method we assume that emissions in counties adjacent to and/or upwind of the Chicago/Gary MSA do not significantly contribute to the sampled plume.

We also assume that the annual emissions are representative of emissions on each day of sampling. We acknowledge the limitations of this assumption, as source emissions may vary diurnally,

seasonally, and from weekday to weekend. The flight in question took place on a Sunday in summer, and the EmRs determined from the annual inventory may differ from the actual emissions on this particular day and time. While it is possible to examine facility-level databases with higher temporally-resolved emissions, this would not have allowed us to include nonpoint and onroad or nonroad mobile source emissions, which contribute substantially (albeit to varying degrees) to the four pollutants of interest. Therefore, in an effort to incorporate all inventoried source emissions for THg, SO_2, NO_x, and CO, we determined that the annual EPA NEI was the most applicable resource and one that requires validation.

2.7. Emission ratios (EmRs)

We use FLEXPART to derive spatially appropriate emission ratios for our analysis. The footprint analysis combines air mass residence time (s m^3 kg^{-1}) in the model grid cells with emission fluxes (kg m^{-3} s^{-1}) to determine the emission contribution to the sampled air mass. To determine the air mass residence time in a given volume of air, we multiply the horizontal dimensions of the output grid (0.2° by 0.2°, or approximately 20 km by 20 km) by the planetary boundary layer (PBL) height, which we approximate to be 2000 m above sea level (ASL) using the nearest upper air sounding at 0 UTC on July 8, 2013. Emission fluxes are determined from annual emissions in the 2011 NEI (see Section 2.6). We determine the area of each county using the sum of land and water areas in the TIGER/Line Shapefile database (U.S. Census Bureau, 2013). At each hour along the back-trajectory, residence time fields are multiplied by gridded emission fluxes to give a mass mixing ratio per county that would be measured at the receptor (the C-130 aircraft). We sum these mass mixing ratios across all hours and all counties, and convert them to volume (molar) mixing ratios. We acknowledge that this FLEXPART analysis is based on global-scale gridded meteorology (Section 2.4) which provides a lower resolution representation of transport in this regional-scale feature. However, as the non-point source emissions are reported on a county-wide basis (Section 2.4), combining these emissions with a global-scale meteorological model is consistent and represents the most appropriate method given the spatial resolution of the emissions dataset.

We calculate NO_x and SO_2 losses during transport from source to receptor following the method of Ambrose et al. (2015), assuming that losses are governed by reaction with OH. We neglect loss of SO_2 in cloud droplets based on minimal cloud cover and low relative humidity (RH), as shown in satellite imagery and upper air maps and as indicated by moderate RH observed from the C-130 over Lake Michigan (average RH 63%). This assumption is also appropriate for NO_x as this was a daytime flight and thus oxidation by OH would dominate over reaction with ozone to form N_2O_5. This method requires knowing the transport time, which we derive using the distance and local wind speed between the source and receptor location. We consider the receptor location to be the C-130 position at the peak of the plume encounter. We use the FLEXPART-modeled air mass path and assume the center of Chicago/Gary to be the confluence of Cook, Will, and DuPage counties in Illinois. While this is an approximate source location, we find that adjusting the source-receptor distance over the range of values along the path of the local wind direction does not significantly change the resulting EmRs. We find the lifetime of NO_x against reaction with OH in the two subsequent plume crossings to be 2.7 h (81% removal) and 3.4 h (61% removal), respectively. Similarly, we find the lifetime of SO_2 against reaction with OH in each plume crossing to be 26 h (16% removal) and 34 h (9% removal), respectively. We assume no loss of THg or CO during the 3–5 h of transport time.

We use the resulting FLEXPART output to determine EmRs representative of the enhancement due to emissions from the Chicago/Gary urban/industrial area. We acknowledge that to compare these inventoried EmRs to the observed ERs we must assume that the plume is well-mixed, given that the predominant emissions of THg, CO, NO_x, and SO_2 come from different source sectors. We characterize uncertainty in the EmRs based upon reported uncertainties in the FLEXPART back-trajectory calculations as follows: Angevine et al. (2014) estimated 30–40% variation in surface residence times for typical meteorological conditions. Brioude et al. (2012) showed that using instantaneous instead of time-averaged wind fields adds ~10%. Brioude et al. (2011), using three different meteorological input datasets including the NCEP GFS, concluded that uncertainty introduced to meteorology is ~20%. Considering this information, we conservatively estimate the uncertainty in our model simulations due to particle dispersion calculations to be ±40%, which we apply to the EmRs in Table 1. Characterizing the uncertainty due to parameterizations employed within the model is very challenging and beyond the scope of this paper.

3. Results and discussion

3.1. Summary of airborne measurements

On July 7, 2013, the C-130 departed Smyrna, TN, at approximately 15:00 UTC (11:00 a.m local time) and traveled northward toward the Chicago/Gary urban/industrial area. The aircraft began descending from 4255 m ASL into the boundary layer at 16:20 UTC, approximately 135 km south of the Lake Michigan shoreline. We collected measurements over the lake at a flight altitude of less than 1000 m ASL for approximately 3 h (Figs. 2–3). We first intercepted the Chicago/Gary plume between 18:42:30 and 18:47:30 UTC when the C-130 was over the southernmost portion of the lake and approximately 120 km east-northeast of the Chicago urban area center (approximately 75 km east-northeast of the shoreline, following the same heading) (Fig. 2). The C-130 circled back to sample this plume a second time at 18:55 UTC approximately 100 km east-northeast of the urban area's center. The flight altitude was below 500 m ASL at both times. The THg mixing ratios during the two plume passages were 219 ppqv and 208 ppqv, respectively, well above the average of 178 ppqv observed over Lake Michigan outside of these two plume crossings. We detected concurrent enhancements in CO (794 ppbv and 540 ppbv, respectively), SO_2 (14.5 ppbv and 5.9 ppbv, respectively), and NO_x (6.6 ppbv and 2.4 ppbv, respectively) (Fig. 4). We note that in the first passage, the NO_x and SO_2 maximums are offset from the CO maximum by 100 s, whereas during the second passage the maximums in the three species occur simultaneously. FLEXPART 72-h back-trajectories during these subsequent plume encounters depict southwesterly transport across the Chicago-Gary urban/industrial area (Fig. 4).

Airborne observations of VOCs confirm the influence of urban/industrial emissions on the sampled plume. Across the two plume encounters, an RMA regression of i-pentane to n-pentane observations has a slope of 1.73 pptv/pptv, where a ratio between 1.5 and 2.0 is indicative of an urban atmosphere with a mixture of vehicular emissions (Baker et al., 2008). The RMA regression of i-butane to n-butane has a slope of 0.60, which also indicates urban emissions (Baker et al., 2008). Additionally, tetrachloroethene (C_2Cl_4), a manufactured chemical and urban/industrial tracer (Simpson et al., 2004), was elevated (>4 pptv) above the North American background for most of the period between 18:00–19:00 UTC, with mixing ratios of 5.54 pptv and 4.95 pptv during the two plume crossings. These observations corroborate the influence of Chicago/Gary emissions in the plume encounters.

Table 1
Measured enhancement ratios (ERs) determined during the two plume crossings downwind of the Chicago/Gary urban/industrial area, and comparison between measured ERs and the inventoried emission ratios (EmRs) obtained from the FLEXPART footprint analysis. Plume A corresponds to the first plume crossing (18:37:30 to 18:50:00 UTC), and Plume B corresponds to the second plume crossing (18:52:30 to 19:02:30 UTC). Regressions for "A & B" use data points from both crossings combined (18:37:30 to 19:02:30 UTC). Plumes A1 and A2 correspond to measurements from 18:37:30 to 18:44:30 UTC and from 18:44:40 to 18:52:20, respectively, and they are compared to the EmRs determined for plume A in the table below. All of the measured ER correlations are significant ($p < 0.05$) except THg/NO_x in plume crossing B. The EmR correction accounts for loss of NO_x and SO_2 during transport.

Plume crossing	THg/CO	THg/NO_x	THg/SO_2	NO_x/CO	SO_2/CO	NO_x/SO_2
	Measured ER ($\times 10^{-6}$ mol mol^{-1}) (r^2, n)			**Measured ER (mol mol^{-1}) (r^2, n)**		
A & B	0.21 ± 0.09 (0.84, 11)	20 ± 11 (0.83, 10)	6.4 ± 3.5 (0.78, 11)	0.011 ± 0.003 (0.33, 130)	0.029 ± 0.009 (0.41, 155)	0.37 ± 0.10 (0.88, 130)
A	0.20 ± 0.15 (0.80, 6)	19 ± 13 (0.88, 6)	5.8 ± 4.5 (0.83, 6)	0.012 ± 0.004 (0.30, 79)	0.033 ± 0.011 (0.40, 90)	0.36 ± 0.10 (0.87, 79)
A1	N/A	N/A	N/A	0.006 ± 0.002 (0.76, 42)	0.018 ± 0.005 (0.87, 43)	0.35 ± 0.11 (0.88, 42)
A2	N/A	N/A	N/A	0.021 ± 0.008 (0.47, 37)	0.056 ± 0.020 (0.60, 47)	0.38 ± 0.12 (0.85, 37)
B	0.22 ± 0.13 (0.93, 5)	29 ± 33 (0.94, 4)	13 ± 2.2 (0.98, 5)	0.007 ± 0.002 (0.82, 51)	0.015 ± 0.004 (0.85, 65)	0.45 ± 0.13 (0.94, 51)
	$EmR_{corrected}$ ($\times 10^{-6}$ mol mol^{-1})			**$EmR_{corrected}$ (mol mol^{-1})**		
A	0.12 ± 0.05	7.1 ± 2.8	3.2 ± 1.3	0.017 ± 0.007	0.037 ± 0.015	0.45 ± 0.18
B	0.13 ± 0.05	3.7 ± 1.5	2.8 ± 1.1	0.036 ± 0.015	0.049 ± 0.019	0.75 ± 0.30
				% Difference ER vs EmR		
A	67%	171%	81%	−32%	−13%	−21%
A1	N/A	N/A	N/A	−64%	−52%	−24%
A2	N/A	N/A	N/A	25%	50%	−16%
B	63%	681%	355%	−82%	−70%	−41%

Although we sampled over Lake Michigan during earlier and later segments of the flight, prior to 17:45 UTC and after 19:00 UTC the C-130 flight altitude was above 500 m ASL and the concentrations of THg and other trace gases were substantially lower (Fig. 3). This suggests that the plume we sampled at 18:45 and 18:55 UTC was concentrated in a low-level layer over the lake. Additionally, during segments of the flight when the C-130 was sampling further north over central Lake Michigan, the trajectories corresponding to smaller enhancements in THg, CO, NO_x, and/or SO_2 (Fig. 3) depict westerly flow from areas along the western Lake Michigan shoreline that are north of the urban/industrial area; thus the air sampled at those times was less influenced by Chicago/Gary and likely more influenced by individual sources along the shoreline (Fig. 2) or by other smaller urban areas.

3.2. Measured ERs

Fig. 5 and Table 1 show the RMA regressions of THg versus CO, NO_x, and SO_2 using measurements across the two previously described plume crossings. Due to the 2.5-min sampling frequency of the DOHGS instrument, we first report the THg-based regressions across the two plume crossings together (18:37:30 to 19:02:30 UTC) to increase the number of data points in the regression (Fig. 5). We find the THg/CO ER to be 0.21 (±0.09) × 10^{-6} mol mol^{-1} (ppqv/ppbv). The THg/NO_x ER is 20 (±11) × 10^{-6} mol mol^{-1}, and the THg/SO_2 ER is 6.4 (±3.5) × 10^{-6} mol mol^{-1}. We also provide these regressions for each plume crossing separately (where "A" is the crossing from 18:37:30 to 18:50:00 UTC and "B" is the crossing from 18:52:30 to 19:02:30 UTC, as shown in Fig. 5). We find the THg/CO ER to be

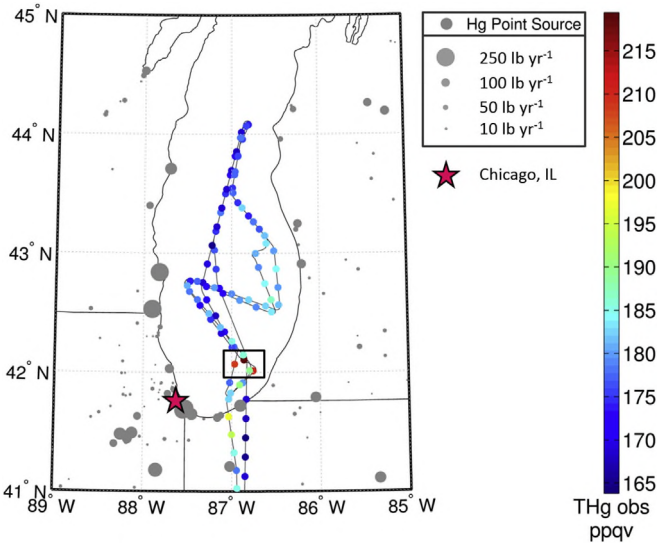

Fig. 2. C-130 flight track over Lake Michigan during RF-15 on July 7, 2013. The flight track is color coded by the measured THg concentration onboard the C-130. The gray circles correspond to point sources emitting more than 0.5 lb yr^{-1} (0.00025 tpy) of Hg. The black box identifies observations made during the Chicago/Gary plume crossing. (For interpretation of the references to colour in this figure legend, the reader is referred to the web version of this article.)

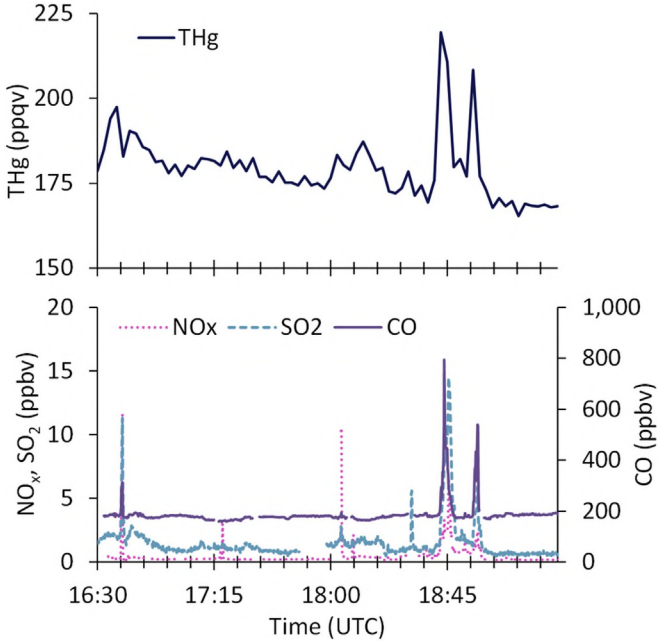

Fig. 3. Time series of THg, NO_x, SO_2, and CO observations over Lake Michigan from 16:30:00 to 19:30:00 UTC during NOMADSS RF-15 on July 7, 2013.

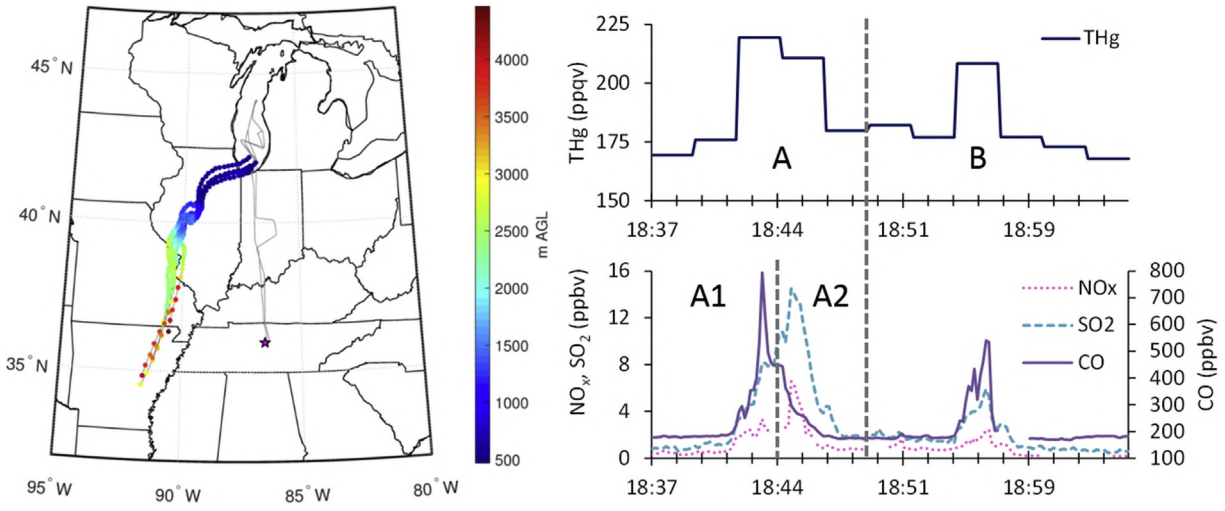

Fig. 4. **(a)** FLEXPART 72-h back-trajectories initiated along the C-130 flight track during RF-15 from 18:40 to 18:55 UTC. Trajectory cluster centers (Stohl et al., 2002) are color-coded by altitude in meters above ground level (m AGL). **(b)** Measured mixing ratios of THg, CO, NO_x, and SO_2 over Lake Michigan during RF-15; we intercepted the Chicago/Gary plume at approximately 18:45 UTC and 18:55 UTC. (For interpretation of the references to colour in this figure legend, the reader is referred to the web version of this article.)

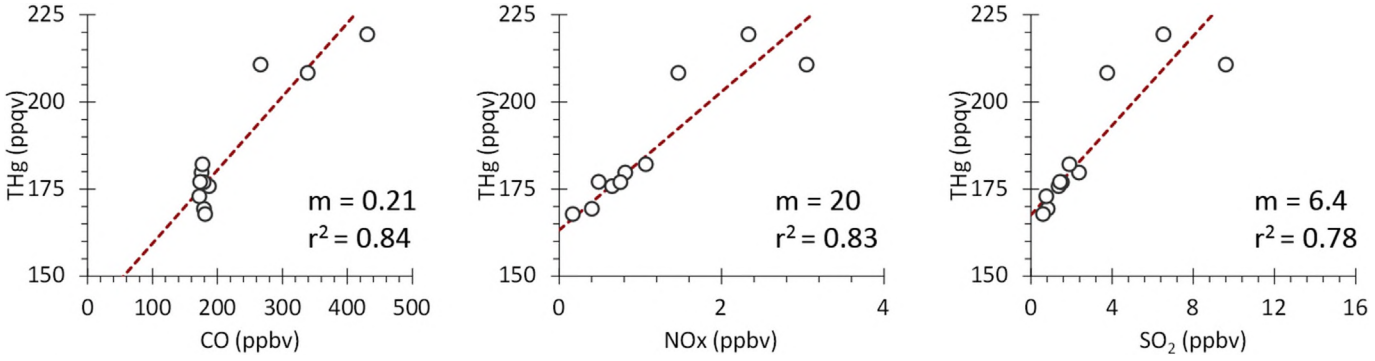

Fig. 5. Mercury enhancement ratios (ERs) determined from measurements made onboard the C-130 between 18:37:30 and 19:02:30 UTC (plumes A + B) downwind of the Chicago/Gary urban area. Slopes and r^2 values were determined from reduced major axis (RMA) regressions and are also shown in Table 1.

consistent to within estimated uncertainties across the two plume crossings, whereas the THg/NO_x and THg/SO_2 ERs show substantial variability between crossings A and B (Table 1). This points to in-plume variability in the concentrations of NO_x and SO_2, suggesting that the plumes were not as well-mixed with respect to these species. We note that all of the measured ER correlations are statistically significant ($p < 0.05$), with exception of THg/NO_x in plume crossing B whose insignificant ER may be due in part to the smaller number of data points ($n = 4$) for that regression (Table 1).

We similarly provide ERs for each of the co-pollutants (NO_x/CO, SO_2/CO, and NO_x/SO_2). A single regression analysis for the two plume crossings (A + B) results in ERs for NO_x/CO, SO_2/CO, and NO_x/SO_2 of 0.011 ± 0.003, 0.029 ± 0.009, and 0.37 ± 0.10 mol mol^{-1}, respectively. However, because we have 10-s observations of CO, NO_x, and SO_2, we have sufficient data to examine each plume crossing separately for these species. For the first plume crossing, we also divide the plume into two segments ("A1": 18:37:30 to 18:44:30 UTC, and "A2": 18:44:40 to 18:52:20) following the offset of the NO_x and SO_2 maximums from the CO maximum (Fig. 5). We find that the NO_x/CO and SO_2/CO enhancements in plumes A1 and B are statistically equivalent to one another, and we propose that these ER values are representative of the Chicago/Gary plume (Table 1). We propose that plume A2 has an enhanced contribution from a particular source or source sector causing the regressions to differ from plumes A1 and B. Nonetheless, the THg/CO ERs appear to be uniform across the plumes within our ability to quantify them.

3.3. *Inventoried EmRs determined from FLEXPART footprint analysis*

Table 1 also summarizes the EmRs obtained from the FLEXPART footprint for plume crossings A and B, and shows the comparison to measured ERs. The percent difference between each ER and EmR is reported with respect to the EmR, and values are negative when the ER is less than the EmR. We find that the measurement-based THg ERs are consistently higher than the modeled THg EmRs. Specifically, for the two plume crossings the observed THg/CO ERs are 63% and 67% greater than the inventoried EmRs. The differences between EmRs and ERs for THg/NO_x and THg/SO_2 during plume crossing A are 171% and 81%, respectively, whereas for plume crossing B the differences are substantially larger (681% and 355%, respectively; Table 1). In contrast, the ERs and EmRs for the co-pollutant ratios (NO_x/CO, SO_2/CO and NO_x/SO_2) are generally in better agreement for both plume crossings, with most ERs slightly lower than the EmRs (Table 1). This agreement between the co-pollutant ERs and EmRs supports our assumption that the annual emissions inventory is representative of our observations during the period in question. Thus, based on this analysis suggesting that

the inventory is accurate for emissions of CO, NO_x, and SO_2, we can conclude that the inventory is biased low for THg emissions.

It is plausible that upwind sources along the trajectory path (such as in Peoria, IL, Springfield, IL, and St. Louis, MO, which have been shown to contribute to Hg wet deposition in Chicago (Gratz et al., 2013b)) may have contributed to outflow from the Chicago/Gary area; however, in that event we would expect emissions from those regions to also be reflected in the co-pollutant ERs and lead to a substantial positive bias with respect to the co-pollutant EmRs, which we did not observe. We also recognize that any THg emitted as Hg^{II} from Chicago/Gary could have been deposited between the source and receptor locations, but we assume this is not a significant contribution to our observations, and therefore to the underestimate in emitted THg, given the relatively short distance between the C-130 and the Chicago/Gary urban/industrial area center (~120 km) and the lack of precipitation on this day that could have removed Hg^{II} by wet deposition. Furthermore, while previous inventories estimated up to 50% of THg emissions in CFPP plumes to be Hg^{II}, recent observations suggest that this fraction is significantly lower (Kos et al., 2013), which supports our expectation of minimal loss through deposition. Lastly, any loss of Hg^{II} (if it occurred) upwind of the C-130 would only exacerbate the calculated ER vs EmR differences, as such losses would depress the effective EmRs.

Ambrose et al. (2015) showed that EmRs derived from the NEI for six CFPPs in the southeastern U.S. were strongly correlated with measured ERs for those facilities, but that the inventory tended to underestimate CFPP Hg emissions with an overall 39% low bias. Assuming that this bias is broadly applicable to CFPPs in the NEI, this is one factor that could contribute to the difference between observed ERs and inventoried EmRs for the Chicago/Gary area. We test this in our FLEXPART simulation by increasing Hg emissions by 39% in the coal combustion for electricity generation category. This reduces the difference between the THg/CO ERs and EmRs to 51% and 46% for plume crossings A and B, respectively. The ER versus EmR differences for THg/NO_x and THg/SO_2 are similarly reduced to 145% and 63% for crossing A and 598% and 307% for crossing B. The remaining difference is likely due to sources which are either not fully accounted for or are simply not included in the inventory. This could include multiple smaller sources in this highly industrialized area that collectively emit substantial THg. Re-emission of legacy Hg from the terrestrial surface may also be a significant source of THg to the local atmosphere, particularly in summer under more direct solar radiation and the absence of snowpack, as has been observed in the vicinity of large point sources (Eckley et al., 2013). Considering our summertime measurements and given that legacy emissions are not included in the EPA NEI, this is one factor that may be responsible for the offset between measured ERs and inventoried EmRs. Lastly, Zhang et al. (2016) showed that the use of Hg in commercial products (also not accounted for in the inventory) comprises more than 50% of annual anthropogenic Hg emissions in North America, perhaps further contributing to the underestimate in THg emissions from urban areas like Chicago/Gary.

3.4. Comparison to THg/CO ERs for other urban/industrial areas

A small number of airborne, cruise, and ground-based campaigns have quantified the outflow of atmospheric Hg from major source regions and similarly determined the Hg/CO ER for those locations (Friedli et al., 2004; Jaffe et al., 2005; Radke et al., 2007; Talbot et al., 2008; Weiss-Penzias et al., 2006, 2013) (Table 2). We find that our observed THg/CO ER downwind of Chicago/Gary is comparable to values reported downwind of Los Angeles, CA (Radke et al., 2007; Weiss-Penzias et al., 2013). In contrast, the THg/CO ER for Chicago/Gary is significantly lower than values reported for outflow from East Asia (Friedli et al., 2004; Jaffe et al., 2005; Weiss-Penzias et al., 2006). This is reasonable given the much higher Hg emissions from coal-combustion in Southeast Asia. Similar to our observations from Chicago/Gary, Weiss-Penzias et al. (2013) found using shipborne measurements in the Los Angeles urban outflow that the inventoried Hg/CO ratio was biased low compared to observations, and suggested that there is a larger source of Hg to the atmosphere in this urban area than what is accounted for in the inventory. In summary, our results, together with those of Weiss-Penzias et al. (2013), imply that THg emissions from U.S. urban/industrial regions are under-estimated.

4. Conclusion

Previous ground-based studies in the Chicago/Gary area showed that local emissions significantly contribute to Hg deposition and elevated ambient Hg concentrations in the region. Our airborne observations have directly quantified the chemical composition of the Chicago/Gary plume and the enhancement of THg over background levels. These results confirm that, even with the recent implementation of the MATS and the corresponding reductions in CFPP Hg emissions, the Chicago/Gary urban/industrial area remains an important source of Hg to the atmosphere over Lake Michigan. Specifically, we find that the EPA NEI underestimates THg emissions in the Chicago/Gary area. We attribute this to a low bias in inventoried CFPP Hg emissions (Ambrose et al., 2015), multiple smaller sources in the highly industrialized area that are not fully accounted for within the inventory, and the absence of legacy Hg and the use of Hg in commercial products from the NEI. It is challenging to quantify the actual THg emission from Chicago/Gary based upon our analyses; however, using the difference between our observed THg/CO ERs (which are comparable with those observed downwind of other urban/industrial areas) and modeled EmRs, we propose that THg emissions may be 65% higher than reported in the NEI, corresponding to annual THg emissions of 1.5 tpy from Chicago/Gary. This difference is well above our method uncertainty of ±40%, confirming the significance of our results. We note that this value

Table 2
Comparison of the THg/CO ER measured during this study with Hg/CO ERs reported downwind of other major urban/industrial areas. Values are reported in units of ppqv/ppbv ($\times 10^{-6}$ mol mol^{-1}).

Location	Study	Hg/CO (x 10^{-6} mol mol^{-1})
Shanghai, China	Friedli et al. (2004)	0.63 (TGM/CO)
Hedo Station, Okinawa, Japan	Jaffe et al. (2005)	0.62 (±0.17) (GEM/CO)
Asian LRT to U.S. West Coast	Weiss-Penzias et al. (2006)	0.52 (TGM/CO)
LA Basin, CA, U.S.	Radke et al. (2007)	0.20 (GEM/CO)
Anchorage, AK, U.S.	Talbot et al. (2008)	0.66 (±0.05) (GEM/CO)
Honolulu, HI, U.S.	Talbot et al. (2008)	0.37 (±0.07) (GEM/CO)
Mexico City, Mexico	Talbot et al. (2008)	0.30 (GEM/CO; estimated)
LA urban outflow, CA, U.S.	Weiss-Penzias et al. (2013)	0.123 (GEM/CO)
Chicago, IL, U.S.	This Study	0.21 (±0.09) (THg/CO)

would reflect all source emissions, including natural and legacy emissions as well as the anthropogenic sources that are in the NEI. To verify this estimation, future work warrants the use of regional-scale chemical transport models with up-to-date Hg emissions estimates and chemistry in order to investigate both transport and processing of emissions within plumes. Higher temporal and spatial resolution in the emission inventory are also needed to better understand the source contributions to observations such as the ones presented here. Lastly, ambient measurements in and downwind of major U.S. urban/industrial areas remain necessary to accurately quantify total emissions of Hg to the local, regional, and global atmosphere.

Data accessibility

Data from the NOMADSS campaign can be obtained through the Southeast Atmosphere Study home page (http://www.eol.ucar.edu/field_projects/sas).

Acknowledgments

The U.S. National Science Foundation provided funding for the NOMADSS project (award #1217010). We thank the staff and scientists from the National Center for Atmospheric Research's Research Aviation Facility for their support throughout the study. We would also like to acknowledge high-performance computing support from Yellowstone (ark:/85065/d7wd3xhc) provided by NCAR's Computational and Information Systems Laboratory, sponsored by the National Science Foundation.

References

Ambrose, J.L., Gratz, L.E., Jaffe, D.A., Campos, T., Flocke, F.M., et al., 2015. Mercury emission ratios from coal-fired power plants in the southeastern United States during NOMADSS. Environ. Sci. Technol. http://dx.doi.org/10.1021/acs.est.5b01755.

Ambrose, J.L., Lyman, S.N., Huang, J., Gustin, M.S., Jaffe, D.A., 2013. Fast time resolution oxidized mercury measurements during the reno atmospheric mercury intercomparison experiment (RAMIX). Environ. Sci. Technol. 47 (13), 7285–7294. http://dx.doi.org/10.1021/es303916v.

Angevine, W.M., Brioude, J., McKeen, S., Holloway, J.S., 2014. Uncertainty in Lagrangian pollutant transport simulations due to meteorological uncertainty from a mesoscale WRF ensemble. Geosci. Model Dev. 7, 2817–2829. http://dx.doi.org/10.5194/gmd-7-2817-2014.

Apel, E.C., Hornbrook, R.S., Hills, A.J., Blake, N.J., Barth, M.C., et al., 2015. Upper tropospheric ozone production from lightning NO_x-impacted convection: smoke ingestion case study from the DC3 campaign. J. Geophys. Res. Atmos. 120, 2505–2523. http://dx.doi.org/10.1002/2014JD022121.

Baker, A.K., Beyersdorf, A.J., Doezema, L.A., Katzenstein, A., Meinardi, S., et al., 2008. Measurements of nonmethane hydrocarbons in 28 United States cities. Atmos. Environ. 42, 170–182.

Brioude, J., et al., 2011. Top-down estimate of anthropogenic emission inventories and their interannual variability in Houston using a mesoscale inverse modeling technique. J. Geophys. Res. 116, D20305. http://dx.doi.org/10.1029/2011JD016215.

Brioude, J., Angevine, W.M., McKeen, S.A., Hsie, E.-Y., 2012. Numerical uncertainty at mesoscale in a Lagrangian model in complex train. Geosci. Model Dev. 5, 1127–1136.

Brooks, S., Ren, X.R., Cohen, M., Luke, W.T., Kelley, P., et al., 2014. Airborne vertical profiling of mercury speciation near Tullahoma, TN, USA. Atmosphere 5 (3), 557–574. http://dx.doi.org/10.3390/atmos5030557.

Driscoll, C.T., Mason, R.P., Chan, H.M., Jacob, D.J., Pirrone, N., 2013. Mercury as a global pollutant: sources, pathways, and effects. Environ. Sci. Technol. 47 (10), 4967–4983. http://dx.doi.org/10.1021/es305071v.

Eckley, C.S., Parsons, M.T., Mintz, R., Lapalme, M., Mazur, M., et al., 2013. Impact of closing Canada's largest point-source of mercury emissions on local atmospheric mercury concentrations. Environ. Sci. Technol. 47 (18), 10339–10348. http://dx.doi.org/10.1021/es401352n.

Friedli, H.R., Radke, L.F., Prescott, R., Li, P., Woo, J.H., et al., 2004. Mercury in the atmosphere around Japan, Korea, and China as observed during the 2001 ACE-Asia field campaign: measurements, distributions, sources, and implications. J. Geophys. Res. Atmos. 109 (D19) http://dx.doi.org/10.1029/2003jd004244.

Gratz, L.E., Keeler, G.J., Marsik, F.J., Barres, J.A., Dvonch, J.T., 2013a. Atmospheric transport of speciated mercury across southern Lake Michigan: influence from emission sources in the Chicago/Gary urban area. Sci. Total Environ. 448, 84–95. http://dx.doi.org/10.1016/j.scitotenv.2012.08.076.

Gratz, L.E., Keeler, G.J., Morishita, M., Barres, J.A., Dvonch, J.T., 2013b. Assessing the emission sources of atmospheric mercury in wet deposition across Illinois. Sci. Total Environ. 448, 120–131. http://dx.doi.org/10.1016/j.scitotenv.2012.11.011.

Gratz, L.E., Ambrose, J.L., Jaffe, D.A., Shah, V., Jaeglé, L., et al., 2015. Oxidation of mercury by bromine in the subtropical Pacific free troposphere. Geophys. Res. Lett. 42, 10494–10502. http://dx.doi.org/10.1002/2015GL066645.

Jaffe, D., Prestbo, E., Swartzendruber, P., Weiss-Penzias, P., Kato, S., et al., 2005. Export of atmospheric mercury from Asia. Atmos. Environ. 39 (17), 3029–3038. http://dx.doi.org/10.1016/j.atmosenv.2005.01.030.

Kos, G., Ryzhkov, A., Dastoor, A., Narayan, J., Steffen, A., et al., 2013. Evaluation of discrepancy between measured and modelled oxidized mercury species. Atmos. Chem. Phys. 13, 4839–4863. http://dx.doi.org/10.5194/acp-13-4839-2013.

Landis, M.S., Keeler, G.J., 2002. Atmospheric mercury deposition to lake Michigan during the lake Michigan mass balance study. Environ. Sci. Technol. 36 (21), 4518–4524. http://dx.doi.org/10.1021/es011217b.

Landis, M.S., Vette, A.F., Keeler, G.J., 2002. Atmospheric mercury in the Lake Michigan basin: influence of the Chicago/Gary urban area. Environ. Sci. Technol. 36 (21), 4508–4517. http://dx.doi.org/10.1021/es011216j.

Lyman, S.N., Jaffe, D.A., 2012. Formation and fate of oxidized mercury in the upper troposphere and lower stratosphere. Nat. Geosci. 5 (2), 114–117. http://dx.doi.org/10.1038/ngeo1353.

Mauldin III, R.L., Frost, G.J., Chen, G., Tanner, D.J., Prevot, A.S.H., Davis, D.D., Eisele, F.L., 1998. OH measurements during the first Aerosol characterization experiment (ACE 1): observations and model comparisons. J. Geophys. Res. 103 (D13), 16713–16729.

Pollack, I.B., Ryerson, T.B., Trainer, M., Parrish, D.D., Andrews, A.E., et al., 2012. Airborne and ground-based observations of a weekend effect in ozone, precursors, and oxidation products in the California South Coast Air Basin. J. Geophys. Res. Atmos. 117, 14. http://dx.doi.org/10.1029/2011jd016772.

Radke, L.F., Friedli, H.R., Heikes, B.G., 2007. Atmospheric mercury over the NE Pacific during spring 2002: gradients, residence time, upper troposphere lower stratosphere loss, and long-range transport. J. Geophys. Res. Atmos. 112 (D19) http://dx.doi.org/10.1029/2005jd005828.

Ridley, B.A., Grahek, F.E., 1990. A small, low flow, high-sensitivity reaction vessel for No chemiluminescence detectors. J. Atmos. Ocean. Technol. 7 (2), 307–311. http://dx.doi.org/10.1175/1520-0426.

Seibert, P., Frank, A., 2004. Source-receptor matrix calculation with a Lagrangian particle dispersion model in backward mode. Atmos. Chem. Phys. 4, 51–63. http://dx.doi.org/10.5194/acp-4-51-2004.

Shah, V., Jaeglé, L., Gratz, L.E., Ambrose, J.L., Jaffe, D.A., et al., 2016. Origin of oxidized mercury in the summertime free troposphere over the southeast United States. Atmos. Chem. Phys. 16, 1511–1530.

Simpson, I., Meinardi, S., Blake, N.J., Rowland, F.S., Blake, D.R., 2004. Long-term decrease in the global atmospheric burden of tetrachloroethene (C_2Cl_4). Geophys. Res. Lett. 31, L08108. http://dx.doi.org/10.2019/2003GL019351.

Song, S., Selin, N.E., Gratz, L.E., Ambrose, J.L., Jaffe, D.A., et al., 2016. Constraints from observations and modeling on atmosphere-surface exchange of merucry in eastern north America. Elementa Sci. Anthr. http://dx.doi.org/10.12952/journal.elementa.000100, 4:000100.

Stohl, A., Hittenberger, M., Wotawa, G., 1998. Validation of the Lagrangian particle dispersion model FLEXPART against large scale tracer experiments. Atmos. Environ. 32, 4245–4264. http://dx.doi.org/10.1016/S1352-2310(98)00184-8.

Stohl, A., Thomson, D.J., 1999. A density correction for Lagrangian particle dispersion models. Bound. Layer Meteorol. 90, 155–167. http://dx.doi.org/10.1023/A:1001741110696.

Stohl, A., Eckhardt, S., Forster, C., James, P., Spichtinger, N., et al., 2002. A replacement for simple back trajectory calculations in the interpretation of atmospheric trace substance measurements. Atmos. Environ. 36 (29), 4635–4648. http://dx.doi.org/10.1016/s1352-2310(02)00416-8.

Stohl, A., Forster, C., Frank, A., Seibert, P., Wotawa, G., 2005. Technical note: the Lagrangian particle dispersion model FLEXPART version 6.2. Atmos. Chem. Phys. 5, 2461–2474.

Swartzendruber, P.C., Jaffe, D.A., Finley, B., 2009. Development and first results of an aircraft-based, high time resolution technique for gaseous elemental and reactive (oxidized) gaseous mercury. Environ. Sci. Technol. 43 (19), 7484–7489. http://dx.doi.org/10.1021/es901390t.

Talbot, R., Mao, H., Scheuer, E., Dibb, J., Avery, M., et al., 2008. Factors influencing the large-scale distribution of Hg degrees in the Mexico City area and over the North Pacific. Atmos. Chem. Phys. 8 (7), 2103–2114.

U.S. Census Bureau - Geography Division, 2013. TIGER/Line® Shapefiles and TIGER/Line® Files. https://www.census.gov/geo/maps-data/data/tiger-line.html.

U.S. Environmental Protectioni Agency (EPA), 2008. Documentation for the 2005 Point Source National Emissions Inventory. Eastern Research Group, Inc., Morrisville, NC, USA. http://www.epa.gov/ttn/chief/net/2005inventory.html#inventorydata.

U.S. Environmental Protection Agency (EPA), 2012. National emission standards for hazardous air pollutants from coal- and oil-fired electric utility steam generating units and standards of performance for fossil-fuel-fired electric utility, industrial-commercial-institutional, and small industrial-commercial-institutional steam generating units. Fed. Regist. 77 (32), 9304–9513.

U.S. Environmental Protection Agency (EPA), 2013. National Emissions Inventory, Version 3, Technical Support Document Draft. U.S. EPA Office of Air Quality Planning and Standards, Air Quality Assessment Division, Emissions Inventory

and Analysis Group, Research Triangle Park, NC, USA, p. 2008. http://www.epa.gov/ttn/chief/net/2008inventory.html.
U.S. Environmental Protection Agency (EPA), 2014a. EPA's Report on the Environment - Mercury Emissions. http://cfpub.epa.gov/roe/indicator.cfm?i=14.
U.S. Environmental Protection Agency (EPA), 2014b. 2011 National Emissions Inventory, Version 1, Technical Support Document Draft. U.S. EPA Office of Air Quality Planning and Standards, Air Quality Assessment Division, Emissions Inventory and Analysis Group, Research Triangle Park, NC, USA. http://www.epa.gov/ttn/chief/net/2011inventory.html.
U.S. Office of Management and Budget (OMB), 2013. Revised Deliniations of Metropolitan Statistical Areas, Micropolitan Statistical Areas, and Combined Statistical Areas, and Guidance on the Uses of the Delineations of These Areas. Bulletin NO. 13–01. Washington, D.C., U.S.
Vette, A.F., Landis, M.S., Keeler, G.J., 2002. Deposition and emission of gaseous mercury to and from lake Michigan during the lake Michigan mass balance study (july, 1994 october, 1995). Environ. Sci. Technol. 36 (21), 4525–4532. http://dx.doi.org/10.1021/es0112184.
Weiss-Penzias, P.S., Jaffe, D.A., Swartzendruber, P., Dennison, J.B., Chand, D., et al., 2006. Observations of Asian air pollution in the free troposphere at Mount Bachelor Observatory during the spring of 2004. J. Geophys. Res. 111, D10304. http://dx.doi.org/10.1029/2005JD006522.
Weiss-Penzias, P.S., Williams, E.J., Lerner, B.M., Bates, T.S., Gaston, C., et al., 2013. Shipboard measurements of gaseous elemental mercury along the coast of Central and Southern California. J. Geophys. Res. Atmos. 118 (1), 208–219. http://dx.doi.org/10.1029/2012jd018463.
Zhang, Y., Jacob, D.J., Horowitz, H.M., Chen, L., Amos, H.M., et al., 2016. Observed decrease in atmospheric mercury explained by global decline in anthropogenic emissions. PNAS 113 (3), 526–531. http://dx.doi.org/10.1073/pnas.1516312113.